NANO LETTERS

pubs.acs.org/NanoLett

Vertically Oriented Sub-10-nm Plasmonic Nanogap Arrays

Hyungsoon Im,[†] Kyle C. Bantz,[‡] Nathan C. Lindquist,[†] Christy L. Haynes,*[,‡] and Sang-Hyun Oh*[,†]

[†]Department of Electrical and Computer Engineering and [‡]Department of Chemistry, University of Minnesota, Minneapolis, Minnesota 55455

ABSTRACT Nanometric gaps in noble metals can harness surface plasmons, collective excitations of the conduction electrons, for extreme subwavelength localization of electromagnetic energy. Positioning molecules within such metallic nanogaps dramatically enhances light−matter interactions, increasing absorption, emission, and, most notably, surface-enhanced Raman scattering (SERS). However, the lack of reproducible high-throughput fabrication techniques with nanometric control over the gap size has limited practical applications. Here we show sub-10-nm metallic nanogap arrays with precise control of the gap's size, position, shape, and orientation. The vertically oriented plasmonic nanogaps are formed between two metal structures by a sacrificial layer of ultrathin alumina grown using atomic layer deposition. We show increasing local SERS enhancements of up to 10^9 as the nanogap size decreases to 5 nm. Because these sub-10-nm gaps can be fabricated at high densities using conventional optical lithography over an entire wafer, these results will have significant implications for spectroscopy and nanophotonics.

KEYWORDS Surface-enhanced Raman scattering, nanogap, surface plasmon, atomic layer deposition, plasmonics

Surface-enhanced Raman scattering (SERS) is a powerful spectroscopic technique that relies on the generation of surface plasmons (SPs)—density fluctuations of the conduction electron plasma[1]—in metallic nanostructures to detect and identify proximate molecules.[2−4] Because of the collective motion of the conduction electrons, SPs can substantially enhance the local electromagnetic (EM) field, while the evanescent nature of the SPs allows their energy to be localized to subwavelength dimensions.[5,6] Illuminating metallic nanoparticles,[7−11] gaps,[12−15] or sharp tips[16−18] can create these subwavelength SERS "hotspots", producing dramatically enhanced Raman signals from adsorbates. The enhanced light−matter interactions in these metallic nanostructures are responsible for SERS as well as many other sensing and imaging applications in the emerging field of plasmonics.[19−21] However, the lack of reproducible high-throughput fabrication methods has limited the widespread adoption of SERS as a general sensing technique.

While the mechanism responsible for single-molecule sensitivity in SERS is not firmly established, it is widely believed that this large enhancement occurs when a SERS-active molecule is positioned within the substantial plasmonic EM fields generated in the gap between two closely spaced metallic nanostructures.[22] Therefore, a large portion of current SERS research is focused toward fabricating nanogap structures via electron-beam lithography,[12] electromigration,[14] nanosphere lithography,[13,23,24] or electrochemical metal growth.[25] In addition, extreme subwavelength confinement of EM energy in nanogaps has critical applications in biosensing, nonlinear optics[26] and plasmonics. However, a reproducible fabrication method, especially one using conventional optical lithography techniques, for the production of sub-10-nm gaps with precise control of the gap's size, position, shape, and orientation remains a significant challenge.

It is well-known that thin film deposition techniques such as physical/chemical vapor deposition and atomic layer deposition (ALD) can provide a level of nanometric precision not achievable by even the most advanced electron-beam lithography. Thin film deposition has been employed to fabricate nanoscale gap or cavity structures with lithography-independent control of the critical dimensions.[27−29] In particular, Miyazaki et al. demonstrated nanometric confinement of visible light in a plasmonic nanocavity where two metal layers were separated by a 3 nm thick SiO_2 layer.[27] However, a major limitation in utilizing such planar structures is the difficulty in coupling normally incident light into and out of the in-plane nanogap. It is problematic to perform Raman spectroscopy over a large array of in-plane nanogaps, since the illumination and collection of the light are shadowed by the metallic overlayers.

Here, this key fabrication challenge is addressed by using ALD—a technique that can readily achieve film thicknesses with subnanometer precision—to form vertically oriented metal−dielectric−metal nanogap structures. Such structures can generate significant field enhancements and tight localization in the gap with normally incident light as shown in Figure 1a. The nanogap fabrication process is illustrated in Figure 1b. A standard lithography technique, such as optical lithography, defines the initial metal pattern. This is followed

* To whom correspondence should be addressed, chaynes@umn.edu and sang@umn.edu.

Received for review: 04/6/2010
Published on Web: 05/25/2010

DOI: 10.1021/nl1012085 | *Nano Lett.* **2010,** *10,* 2231–2236

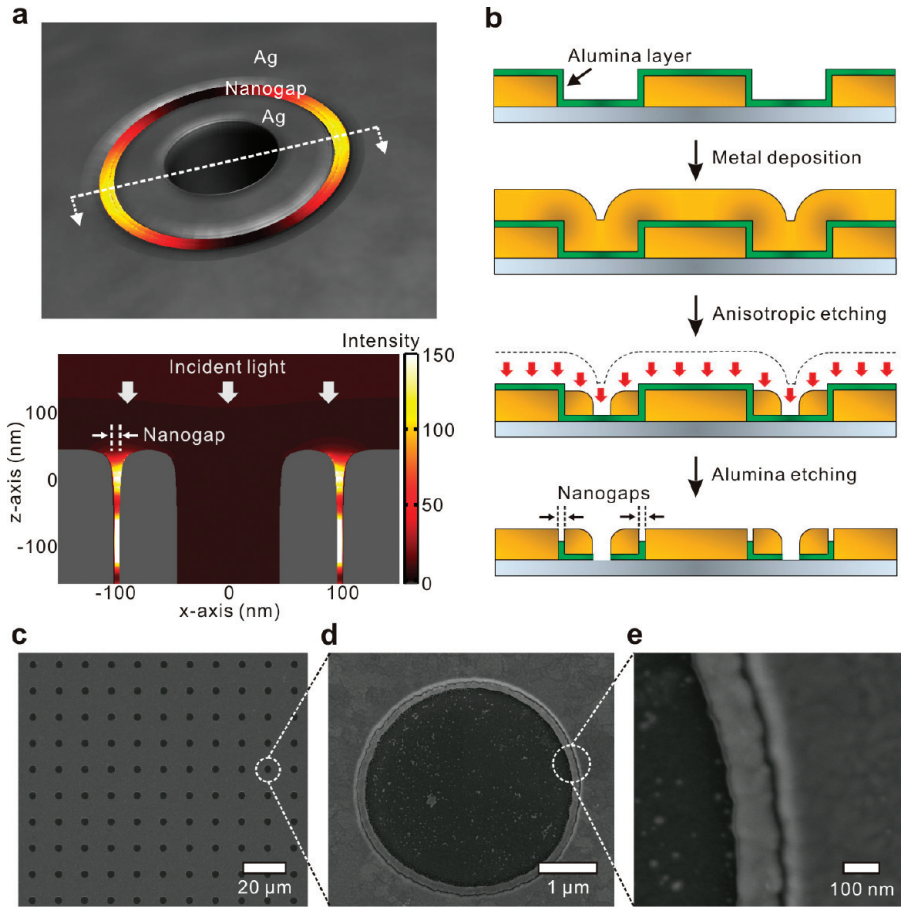

FIGURE 1. (a) 3-D finite-difference time-domain simulation results showing significant field intensity enhancement within a 5 nm nanogap. (b) Fabrication process schematic of the nanogap array. Starting from patterned substrates, the secondary metal layer is separated by a thin alumina spacer deposited using atomic layer deposition. Using sidewall spacer processing, the nanogap size is determined by the thickness of the alumina layer. (c) Scanning electron microscopy (SEM) image of a nanogap array with a circular pattern. (d) The magnified image of a single ring-shaped element shown in panel c. (e) The magnified image of a 10 nm nanogap formed along the ring-shaped element.

by the deposition of an ultrathin sacrificial alumina layer using ALD, which conformally covers the top and vertical sidewall surfaces.[30] After the deposition of a second metallic layer, anisotropic ion milling is performed to create metallic sidewalls spaced by the now-exposed alumina. The nanogaps are formed by partially removing the alumina layer with a buffered oxide etchant. In this process, the critical dimension of the nanogap structure is precisely determined by the thickness of the conformal alumina layer, which, in our structures, ranges from 5 to 20 nm. A continuous nanometric gap is created along the perimeter of the patterned metal areas, providing a wide variety of design freedom for making SERS substrates and plasmonic devices such as waveguides and resonators.[31] Figure 1c–e shows a circular gold–air–silver nanogap array, where the circles were defined using optical lithography over a 4-in. Si wafer. Each circle in the gold film contains a 10 nm nanogap structure along its inner wall. By use of photoresist with opposite polarity, inverse structures were also made (Supplementary Figure S1 in Supporting Information). Various other silver–air–silver nanogap structures, where the initial patterns were defined using focused ion beam milling, are shown in Figure 2. The key advantage of this fabrication scheme is the ability to confine and manipulate SPs and their associated high field intensities along the entire vertically oriented metal–air–metal nanocavities.[31]

To characterize the SERS performance of the silver–air–silver nanogap arrays, substrates were incubated in 1 mM benzenethiol (BZT), a well-characterized and efficient Raman scatterer. Ag film over nanosphere (AgFON) substrates,[32] which have been widely used for SERS applications, were used as reference samples. On the AgFON substrates, the field distribution varies with position, where only a few dominant Raman "hotspots" contribute to the overall signal.[33] In contrast, with our structures, it is possible to generate well-defined, high-density hotspots along the entire length of the nanogap.

For a quantitative comparison, confocal Raman microscopy was used to map the spatial distribution of hotspots and to calculate SERS enhancement factors from several substrates. A diffraction-limited 514.5 nm laser spot was scanned over the substrates, and Raman spectra were collected as a function of position. Each pixel in the Raman intensity images was generated by calculating the height of

DOI: 10.1021/nl1012085 | *Nano Lett.* **2010,** *10,* 2231–2236

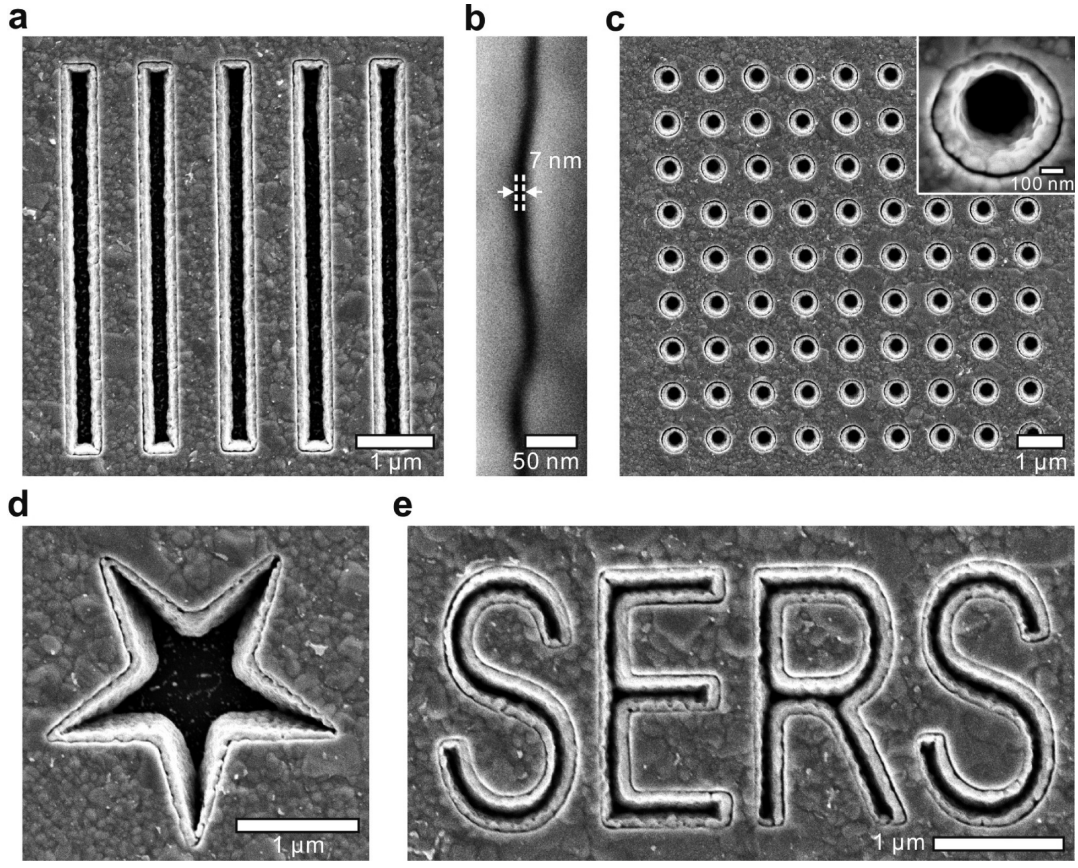

FIGURE 2. Scanning electron microscope images of different types of nanogap arrays: (a) slit array with 500 nm width and 1.5 μm periodicity; (b) the magnified image of 7 nm nanogap from a slit pattern shown in panel a; (c) 9 × 9 nanohole array with 500 nm diameter, the inset to panel c shows the magnified image of one of holes; (d) nanogap on a single star-shaped substrate; (e) nanogap formed along a "SERS" character pattern.

the band at 1,075 cm^{-1} shift, an aromatic breathing mode in BZT. While an 8 × 8 μm^2 area of an AgFON substrate shows randomly distributed hotspots (Figure. 3a), a nanogap device made on a periodic nanohole pattern with an ALD-defined gap size of 5 nm shows a more homogeneous distribution of hotspots with stronger Raman signals for the same incident laser power covering the same area (Figure 3b). We chose the nanohole periodicity (500 nm) to give high nanogap density, but spaced far enough apart to resolve individual nanogap hotspots with our excitation laser wavelength (514.5 nm). While not presented here, the array periodicity may be further optimized for resonant operation. The Raman intensity images were then filtered according to a specific spatially averaged enhancement factor (EF) threshold (Figure 3a,b, panels 1−4; also see Supporting Information for EF calculations). Clearly, the nanogap device has a significantly higher density of hotspots with a spatially averaged EF above 1 × 10^5 and 2 × 10^5 (panels 3 and 4, respectively) than does the AgFON substrate (panels 1 and 2, respectively). Indeed, less than 30% of the AgFON substrate has spatially averaged EFs above 1 × 10^5, while the nanogap sample shows more than 90% coverage. This drops only slightly when the threshold is raised to 5 × 10^5, whereas less than 1% of the AgFON area exceeds this EF (Figure 3c). Additionally, the ALD-defined nanogaps exhibit a signal-to-background contrast of more than 500 between nanogap and non-nanogap areas (Figure 3d). It should be noted that the nanogap EFs calculated here are spatially averaged over the spot size of the incident laser (Supplementary Figure S3 in Supporting Information), and the local EF along the nanometer gap itself is much higher, as explained below.

With these metallic nanogap structures, the SERS intensity is maximized when the incident light is polarized across the gap and minimized when the polarization is parallel to the gap.[34,35] Our 10 nm gap devices exhibit the expected polarization dependence, since the number of hotspots decreases by more than 2-fold when the incident polarization is switched parallel to the nanogap (Figure 4a). Since the lithographically defined sidewall exhibits its own nanoscale roughness (Figure 2b), some hotspots will still remain. With square patterns, it is also clear that the SERS hotspots are redistributed according to the incident polarization (Figure 4b). In Figure 4c, with a vertical polarization, the nanogap areas marked as "1" are aligned perpendicular to the incident polarization and show a signal intensity approximately three times higher than the orthogonal regions "2". This is reversed with horizontal polarization.

DOI: 10.1021/nl1012085 | *Nano Lett.* **2010,** *10,* 2231–2236

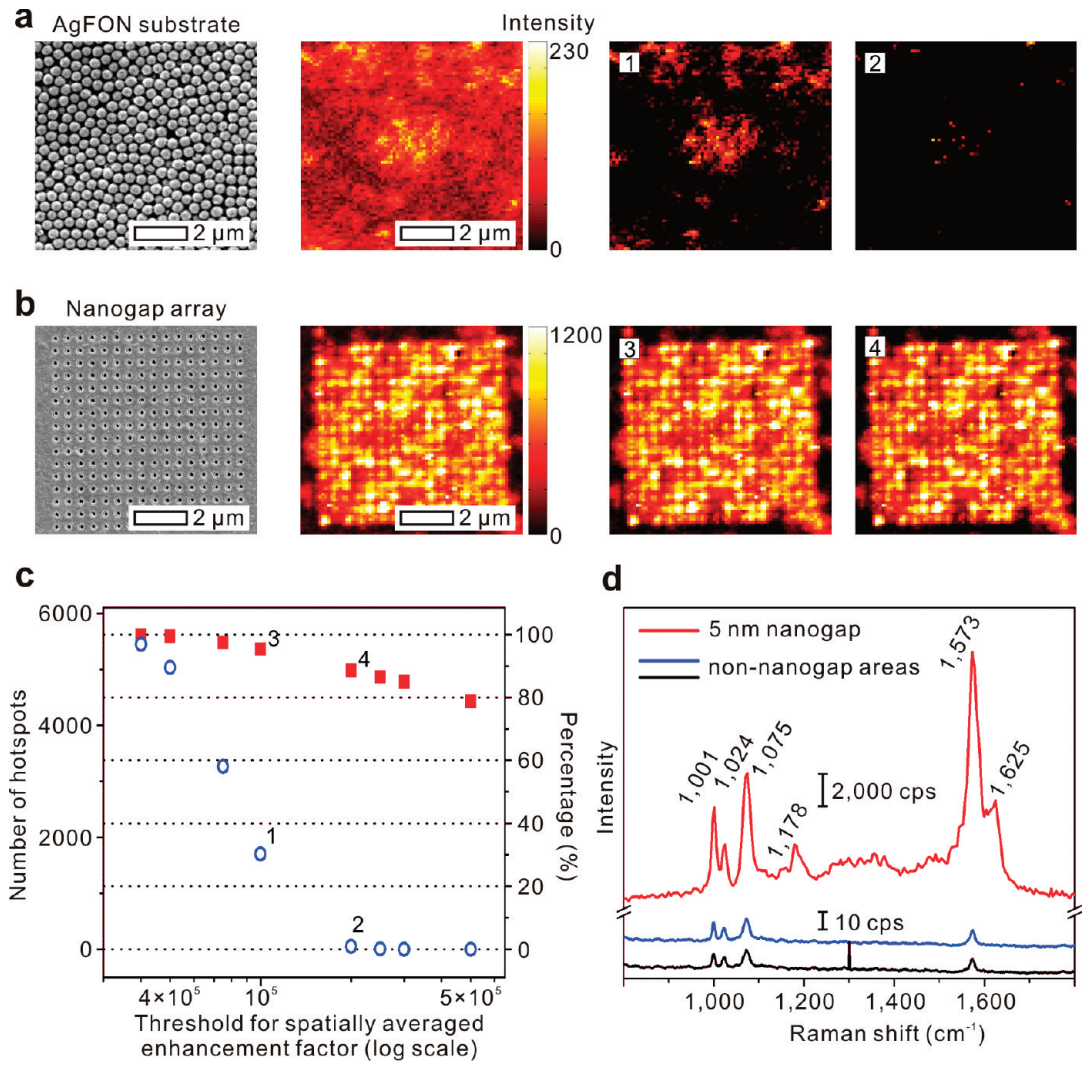

FIGURE 3. (a) Confocal Raman imaging of a Ag film over nanosphere (AgFON) substrate and (b) nanogap array of hole patterns with different spatially averaged EF thresholds (1×10^5 and 2×10^5 in panels 1 and 3 and 2 and 4, respectively). (c) The number and percentage surface coverage of SERS hotspots above various EF thresholds. Open circles are measurements from AgFON substrates while closed squares are measurements from nanogap arrays. The numbers (1, 2, 3, and 4) refer to representative images in panels a and b. (d) Comparison of Raman spectra of benzenthiol from nanogap (red line) and non-nanogap (blue and black lines) areas.

With the 5 nm gap structures studied here, the gap size, rather than the specific shapes of the initial lithographically defined patterns, determines the local EF (Supplementary Figure S4 in Supporting Information). Figure 5 shows the calculated local EFs for various fabricated nanogap structures with different gap sizes ranging from 5 to 20 nm. In this case, local nanogap EFs are calculated based on the assumption that the hotspots are positioned at the edge of the nanogaps, in an area much smaller than the diffraction-limited laser spot size. A very small portion of the adsorbed molecules contribute a disproportionate share of the entire spatially averaged EFs given in Figure 3 (Supplementary Table S1 in Supporting Information). It was experimentally shown that the Raman signal from a non-nanogap area (background) is less than 1% of that from a nanogap area (Figure 3d), supporting the assumption that the SERS signal is coming predominantly from the nanogap regions. A patterned substrate without an ALD step (no nanogap) has spatially averaged EFs less than $\sim 10^5$ (not shown) whereas a 20 nm gap structure has spatially averaged EFs of $\sim 10^6$ and a local EF of $\sim 10^8$. The EF increases as the nanogap size decreases, and a 5 nm gap structure has spatially average EFs above 10^7 with the maximum local EF value exceeding $\sim 10^9$. This behavior of increasing EFs with decreasing gap size is consistent with theoretical calculations.[36]

Together, these results demonstrate high-throughput fabrication of sub-10-nm plasmonic nanogap arrays via the conformal deposition of ultrathin sacrificial layers using ALD on the vertical sidewalls of patterned metal films. The gap size is precisely controlled by the ALD film thickness, and the nanogap is aligned vertically, enabling simple optical excitation and collection over a large area. The position, shape, and packing density of the vertically aligned nanogap structures are determined by an initial metal patterning step.

DOI: 10.1021/nl1012085 | *Nano Lett.* **2010,** *10,* 2231–2236

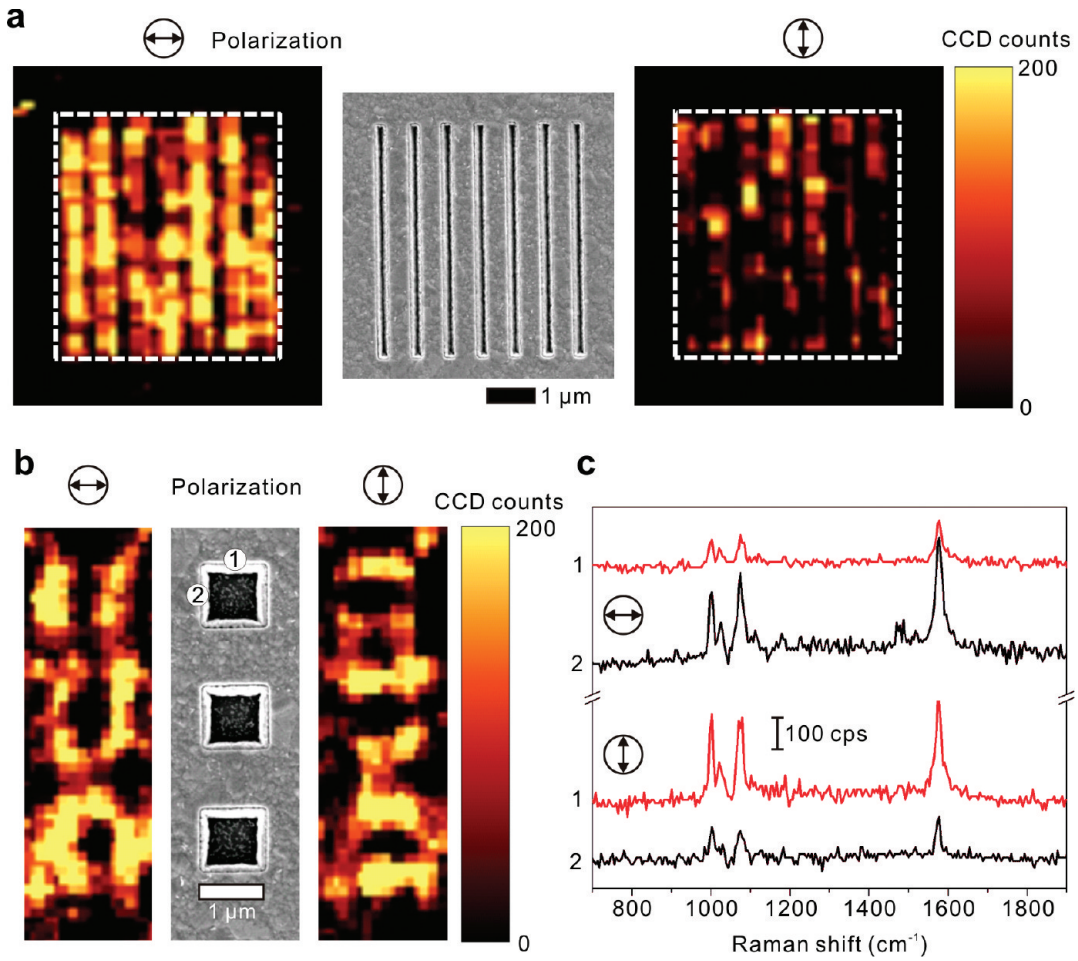

FIGURE 4. (a) Confocal Raman imaging of nanogaps in slit patterns with two different polarization directions of the incident laser beam. (b) Confocal Raman imaging of nanogap in 1 μm $\times$ 1 μm square patterns, showing the modulation of hotspots along the polarization direction. (c) Corresponding Raman spectra from two areas indicated in panel b with two different incident beam polarizations.

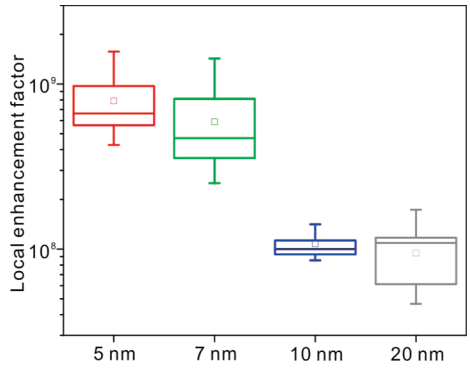

FIGURE 5. The local enhancement factors of nanogap arrays with different nanogap sizes ranging from 5 to 20 nm. Lines in error bars represent values of minimum, 25%, median, 75%, and maximum, and a square represents the mean value.

An array of densely packed 5 nm gaps exhibits high density SERS hotspots with local EFs exceeding 10^9. By combining high-throughput nanofabrication techniques such as nanosphere lithography,[23] nanoimprint lithography,[37] or template stripping,[38] these nanogap structures can be easily and inexpensively fabricated over large areas, opening up many avenues for reproducible and efficient SERS detection. Furthermore, although significant processing challenges remain ahead, if the residual roughness of the patterned metals is eliminated[38] and state-of-the-art ALD techniques are employed to push the limits of our nanogap scheme, it may be possible to make well-defined nanogaps with 1−2 nm gap sizes. Access to plasmonic substrates with large area vertically oriented nanogaps in arbitrary patterns will facilitate control of plasmons and will likely contribute to applications in nonlinear optics,[26] biosensing,[39] and molecular electronics.[40]

Acknowledgment. This research was supported by the NSF MRSEC Program (DMR-0819885), the Minnesota Partnership Award for Biotechnology (H.I., N.C.L., and S.-H.O.), the Camille Dreyfus Teacher-Scholar Fellowship (C.L.H.), and the 3M Faculty Award (S.-H.O.). The team also utilized resources at the University of Minnesota, including the Nanofabrication Center, which receives partial support from NSF through the National Nanotechnology Infrastructure Network, and the Characterization Facility, which has received capital equipment from NSF MRSEC. H.I. and N.C.L.

DOI: 10.1021/nl1012085 | *Nano Lett.* **2010,** *10,* 2231–2236

acknowledge support from 3M Science and Technology Fellowship and the University of Minnesota doctoral dissertation fellowship, respectively.

Supporting Information Available. Detailed descriptions of the fabrication method of the nanogap arrays, fabrication of AgFON substrate, instrumentation, 3-D finite difference time-domain simulation, and SERS enhancement factor calculations and figures showing SEM images of arrays. This material is available free of charge via the Internet at http://pubs.acs.org.

REFERENCES AND NOTES

(1) Ritchie, R. H. *Phys. Rev.* **1957**, *106*, 874–881.
(2) Haynes, C. L.; McFarland, A. D.; Van Duyne, R. P. *Anal. Chem.* **2005**, *77*, 338A–346A.
(3) Jeanmaire, D. L.; Van Duyne, R. P. *J. Electroanal. Chem.* **1977**, *84*, 1–20.
(4) Moskovits, M. *Rev. Mod. Phys.* **1985**, *57*, 783–826.
(5) Genet, C.; Ebbesen, T. W. *Nature* **2007**, *445*, 39–46.
(6) Lal, S.; Link, S.; Halas, N. J. *Nat. Photonics* **2007**, *1*, 641–648.
(7) Kneipp, K.; Wang, Y.; Kneipp, H.; Perelman, L. T.; Itzkan, I.; Dasari, R.; Feld, M. S. *Phys. Rev. Lett.* **1997**, *78*, 1667–1670.
(8) Nie, S. M.; Emory, S. R. *Science* **1997**, *275*, 1102–1106.
(9) Link, S.; El-Sayed, M. A. *Annu. Rev. Phys. Chem.* **2003**, *54*, 331–366.
(10) Nikoobakht, B.; El-Sayed, M. A. *J. Phys. Chem. A* **2003**, *107*, 3372–3378.
(11) Jackson, J. B.; Halas, N. J. *Proc. Natl. Acad. Sci. U.S.A.* **2004**, *101*, 17930–17935.
(12) Gunnarsson, L.; Bjerneld, E. J.; Xu, H.; Petronis, S.; Kasemo, B.; Käll, M. *Appl. Phys. Lett.* **2001**, *78*, 802–804.
(13) Wang, H.; Levin, C. S.; Halas, N. J. *J. Am. Chem. Soc.* **2005**, *127*, 14992–14993.
(14) Ward, D. R.; Grady, N. K.; Levin, C. S.; Halas, N. J.; Wu, Y. P.; Nordlander, P.; Natelson, D. *Nano Lett.* **2007**, *7*, 1396–1400.
(15) Qin, L. D.; Zou, S. L.; Xue, C.; Atkinson, A.; Schatz, G. C.; Mirkin, C. A. *Proc. Natl. Acad. Sci. U.S.A.* **2006**, *103*, 13300–13303.
(16) Stöckle, R. M.; Suh, Y. D.; Deckert, V.; Zenobi, R. *Chem. Phys. Lett.* **2000**, *318*, 131–136.
(17) Neacsu, C. C.; Dreyer, J.; Behr, N.; Raschke, M. B. *Phys. Rev. B* **2006**, *73*, 193406.
(18) Lindquist, N. C.; Nagpal, P.; Lesuffleur, A.; Norris, D. J.; Oh, S. H. *Nano Lett.* **2010**, *10*, 1369–1373.
(19) Barnes, W. L.; Dereux, A.; Ebbesen, T. W. *Nature* **2003**, *424*, 824–830.
(20) Atwater, H. *Sci. Am.* **2007**, *296*, 56–63.
(21) Anker, J. N.; Hall, W. P.; Lyandres, O.; Shah, N. C.; Zhao, J.; Van Duyne, R. P. *Nat. Mater.* **2008**, *7*, 442–453.
(22) Jiang, J.; Bosnick, K.; Maillard, M.; Brus, L. *J. Phys. Chem. B* **2003**, *107*, 9964–9972.
(23) Haynes, C. L.; Van Duyne, R. P. *J. Phys. Chem. B* **2001**, *105*, 5599–5611.
(24) Lu, Y.; Liu, G. L.; Kim, J.; Mejia, Y. X.; Lee, L. P. *Nano Lett.* **2005**, *5*, 119–124.
(25) Gopinath, A.; Boriskina, S. V.; Premasiri, W. R.; Ziegler, L.; Reinhard, B. M.; Dal Negro, L. *Nano Lett.* **2009**, *9*, 3922–3929.
(26) Kim, S.; Jin, J. H.; Kim, Y. J.; Park, I. Y.; Kim, Y.; Kim, S. W. *Nature* **2008**, *453*, 757–760.
(27) Miyazaki, H. T.; Kurokawa, Y. *Phys. Rev. Lett.* **2006**, *96*, 097401.
(28) Kuttge, M.; García de Abajo, F. J.; Polman, A. Nano Lett. **2010**, *10*, 1537–1541.
(29) Lin, J. Y.; Hasan, W.; Yang, J. C.; Odom, T. W. *J. Phys. Chem. C* **2010**, *114*, 7432–7435.
(30) Im, H.; Lindquist, N. C.; Lesuffleur, A.; Oh, S. H. *ACS Nano* **2010**, *4*, 947–954.
(31) Bozhevolnyi, S. I.; Volkov, V. S.; Devaux, E.; Laluet, J. Y.; Ebbesen, T. W. *Nature* **2006**, *440*, 508–511.
(32) Dick, L. A.; McFarland, A. D.; Haynes, C. L.; Van Duyne, R. P. *J. Phys. Chem. B* **2002**, *106*, 853–860.
(33) Fang, Y.; Seong, N. H.; Dlott, D. D. *Science* **2008**, *321*, 388–392.
(34) Xu, H. X.; Käll, M. *ChemPhysChem* **2003**, *4*, 1001–1005.
(35) Baik, J. M.; Lee, S. J.; Moskovits, M. *Nano Lett.* **2009**, *9*, 672–676.
(36) Hao, E.; Schatz, G. C. *J. Chem. Phys.* **2004**, *120*, 357–366.
(37) Chou, S. Y.; Krauss, P. R.; Renstrom, P. J. *Science* **1996**, *272*, 85–87.
(38) Nagpal, P.; Lindquist, N. C.; Oh, S. H.; Norris, D. J. *Science* **2009**, *325*, 594–597.
(39) Im, H.; Huang, X. J.; Gu, B.; Choi, Y. K. *Nat. Nanotechnol.* **2007**, *2*, 430–434.
(40) Song, H.; Kim, Y.; Jang, Y. H.; Jeong, H.; Reed, M. A.; Lee, T. *Nature* **2009**, *462*, 1039–1043.

DOI: 10.1021/nl1012085 | *Nano Lett.* **2010,** *10,* 2231–2236